# An Ab-initio study of Sn-doped $TiO_2$ rutile's optical characteristics, electrical structure, and structural stability at varying doping doses

**Hiba Imane BERREZOUG [1], Zakaria SARI HASSOUN[2], Mohammed BENRAMDANE[3]**

[1] LPT Theoretical Physics Laboratory, Abou-Bekr Belkaïd University, P.O. Box 119, 13000 Tlemcen, Algeria.
[2] MECACOMP, Mechanical Engineering Department, Abou-Bekr Belkaid University, P.O. Box 119 13000 Tlemcen, Algeria.
[3]ETAP Laboratory, Department of Mechanical Engineering, faculty of technology, Abou-Bekr Belkaid University, P.O. Box 119, 13000 Tlemcen, Algeria.

## ABSTRACT

This study investigates the effects of tin (Sn) of doping on the optical, electrical, and structural stability of rutile ($TiO_2$) using the Linearized Augmented Plane-Wave's Complete Potential method combined with Orbitals Local (FP-LAPW+lo), applied using the exchange potential of modified Becke-Johnson (mBJ) and the Density Functional Theory (DFT) framework. The results indicate that Sn doping impacts the lattice parameters and bulk modulus, preserving the structural integrity of $TiO_2$. Pure $TiO_2$ has an energy gap of roughly 2.73 eV, close to the 3.0 eV experimental value. Sn doping raises the optical band gap from 3.13 eV to 3.73 eV because the conduction band minimum has shifted upward. Importantly, no new states emerge within the band gap doping brings. Optical band gap expansion enhances UV absorption and shifts the absorption edge to higher energies, improving solar spectrum utilization. When Sn is doped, UV reflectivity rises, but visible and infrared Reflectivity falls. The energy loss function also shows reduced energy dissipation with higher Sn concentrations. Because of its improved optical and electrical characteristics, Sn-doped $TiO_2$ shows excellent promise as a substitute for indium-doped tin oxide (ITO) in solar cell and photocatalysis applications.

***Keywords:*** *TiO2 rutile, Sn-doped TiO2, FP-LAPW method, mBJ potential, optical properties.*

## 1. INTRODUCTION

Transparent semiconductors are oxides that, in addition to being transparent, can become conductors (type n) if they have excess electrons in their network. These semiconductors are called Transparent Conductive Oxide (TCO). The TCO mainly used is the tin-doped indium oxide (ITO). However, indium is a rare and expensive element, and there will never be enough indium on Earth to consider the mass production of solar cells using an ITO layer. The replacement candidate for the ITO must be an abundant and inexpensive material.

Titanium oxide (TiO2) is an up-and-coming candidate for replacing ITO. It has attracted much attention because of its high stability, efficient solar conversion energy, and inexpensive [1-3]. In addition, TiO2 has interesting applications in gas sensors [4], photo-splitting of water [5], photocatalysis [6], batteries [7] and photovoltaic [8]. When the composition of TiO2 is stoichiometric, it behaves as an insulator, while some defects are enough to make it a semiconductor. Its insensitivity to the lights visible and near-infrared, because of the broadband gap (around 3.2 eV) [9, 10], $TiO_2$ can only absorb light in the near ultraviolet region. The primary applications of $TiO_2$ in thin film form are in solar cells and photocatalytic systems. Titanium oxide is known to crystallize in three distinct phases: Tetragonal P42/mnm rutile, brookite and tetragonal I41/amd anatase. Rutile is nature's most common crystalline phase, while brookite is relatively uncommon. At high temperatures, the rutile phase has the highest thermodynamic stability [11]. In contrast, anatase and brookite are metastable phases that transform rutile when the temperature increases.

The optical absorption edge can be extended toward longer wavelengths by doping $TiO_2$, an easy and effective way to change its optical band gap. This doping increases its photocatalytic effectiveness and improves its solar spectrum utilization [12]. Recently, numerous ionic dopants for TiO2 in different valence states have been studied, such as ($Sb^{5+}$, $Ta^{5+}$, $Nb^{5+}$, $Mo^{5+}$, $Zr^{4+}$, $Sn^{4+}$, $Cr^{3+}$, $Al^{3+}$, $Ga^{3+}$, $Co^{3+}$, $Fe^{3+}$, $Ce^{3+}$, $Ln^{3+}$, $Ca^{2+}$, $Sr^{2+}$ and $Ba^{2+}$) and non-metallic ions such as ($C^{4+}$, $N^{3+}$, $S^{4+}$, $Cl^-$, $Br^-$ and $F^-$) [13-16]. Specifically, TiO2 doped with tin (Sn) is an effective doping and is widely studied. Furthermore, this new molecule swaps the titanium (Ti4+) atoms for tin (Sn4+) atoms. The substitution occurs with slight host structure modification because of their comparable ionic radii. In particular, $Sn^{4+}$ and $Ti^{4+}$ have ionic radii of 0.605 and 0.690 nm, respectively [17].

In this study, we investigate how Sn doping affects the structural electrical and optical characteristics of $TiO_2$ at various concentrations, i.e., $Ti_{1-x}Sn_xO$ (x = 6.25%, 12.5%, and 25% concentrations), using the linearised augmented plane-wave approach with local orbitals for full potential (FP-LAPW+lo), which is formulated within the density functional theory (DFT) framework and incorporates the modified Becke–Johnson (mBJ) exchange potential.

The paper follows this organization: Section 2 describes the theoretical and computational approaches employed; Section 3 concentrates on the findings and discussion; and Section 4 summarises the study along with closing thoughts.

## 2. COMPUTATIONAL DETAILS

This work uses DFT, or density functional theory, which utilizes the optical, electrical, and structural characteristics of Sn-doped $TiO_2$ and pure $TiO_2$. The Kohn-Sham equations' eigenvalues and eigenfunctions were self-consistently determined using the WIEN2k software, incorporating FP-LAPW or linearized augmented plane-wave with a full potential technique [18, 19]. Our computations explore structural properties by applying the Perdew and collaborators technique to the GGA or Generalized Gradient Approximation [20] and electrical and optical characteristics utilizing the approximation of modified Becke-Johnson (mBJ) [21]. We set the Fourier charge density to Gmax = 12 Ry and use a maximum quantum number of $l_{max} = 10$ to describe the expansion of waves within the atomic sphere.

We calculate the self-consistent field (SCF) for total energy with a $10^{-4}$ Ry precision. According to convergence tests, for $TiO_2$ and Sn-doped $TiO_2$, the Brillouin zone's irreducible portion with (100 and 75) k-points is sufficient for accurate total energy minimization. $K_{max}$ denotes the greatest reciprocal lattice vector for creating plane waves. $R_{MT}$ is the shortest muffin-tin radius. The product of these values determines The interstitial region's energy cut-off for plane wave expansions, setting it at 8.5 for $TiO_2$ and 7 for Sn-doped $TiO_2$.
Researchers commonly recognize that a material's dielectric function (ε) defines its electrical and optical characteristics concerning frequency, wavelength, or energy:

$$\varepsilon(\omega) = \varepsilon_1(\omega) + \varepsilon_2(\omega) \quad (1)$$

The dielectric function's imaginary portion, $\varepsilon_2(\omega)$, is acquired straight from computations of the electronic structure [22]:

$$\varepsilon_2(\omega) = (4\pi^2 e^2/\omega^2 m^2)\ \sum_{i,j} \int \langle i[M]j\rangle^2 f_i(1 - f_i)\delta(E_f - E_i\hbar\omega)d^3k \quad (2)$$

(i, j): Initial, End states;
(M) : Dipole;
($E_i$): Energy of electron;
($f_i$): Fermi distribution.

The Kramers-Kronig relation [23] governs the dielectric function's real part:

$$\varepsilon_1(\omega) = 1 + (2/\pi)P \int_0^\infty \omega'\varepsilon_2(\omega')/(\omega'^2 - \omega^2)d\omega' \quad (3)$$

(P): Primary value of the integral.

These two components are used to calculate optical characteristics like the reflectivity R(ω) and absorption coefficient α(ω) [24]:

$$\alpha(\omega) = \omega\sqrt{2}\left[\sqrt{\varepsilon_1^2(\omega) + \varepsilon_2^2(\omega)} - \varepsilon_1(\omega)\right]^{1/2} \quad (4)$$

$$R(\omega) = \left|\sqrt{\varepsilon(\omega) - 1}/\sqrt{\varepsilon(\omega) + 1}\right|^2 \quad (5)$$

This work explores the effects of Sn doping in $TiO_2$ at different concentrations by substituting one Ti atom with one Sn atom. The supercell models considered for 6.25%, 12.5%, and 25% Sn concentrations consist of 48 atoms (2 × 2 × 2 dimensions), 24 atoms (1 × 2 × 2 dimensions), and 15 atoms (1 × 1 × 2 dimensions), respectively (see Figure 1).

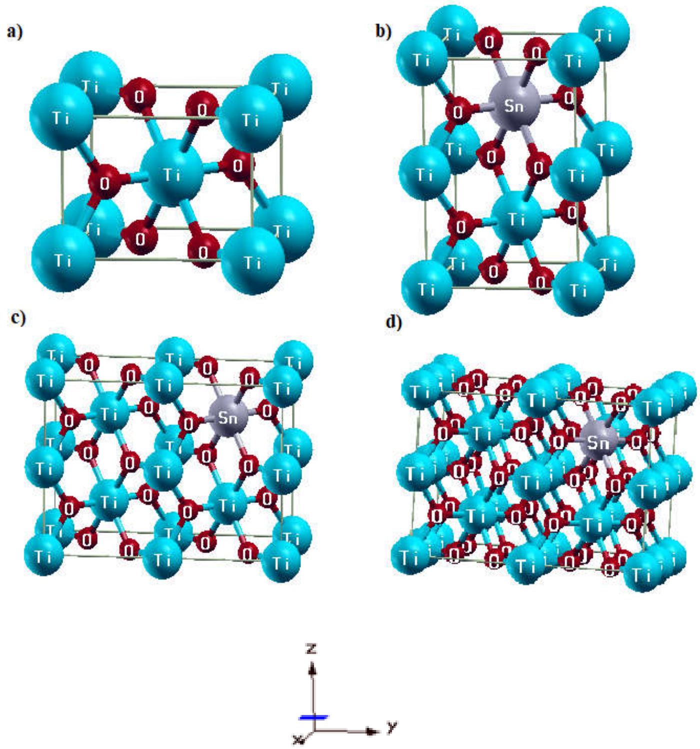

**Figure 1.** Structure of Sn doped TiO2 in: a) pure TiO2, b) supercell (2x1x1) to (25%), c) supercell (2x2x1) to (12.5%), d) supercell (2x2x2) to (6.25%).

## 3. DISCUSSION OF CALCULATED RESULTS

### 3.1. STRUCTURAL PROPERTIES

At normal température, rutile $TiO_2$ displays a tetragonal crystal structure with P42/mnm space group symmetry. Lattice constants: b = a = 4.587 Å c = 2.954 Å, , and angles $\alpha = \beta = \gamma = 90°$ were obtained experimentally [25].

To optimize the lattice parameters for pure and Sn-doped $TiO_2$, we calculate the total energy about the c/a ratio and the unit cell volume. The optimized results, including lattice parameters, pressure derivative, and bulk modulus, are displayed in Table 1.

The calculated parameters for pure $TiO_2$ match well with earlier practical and theoretical investigations [26-30]. As Sn concentration increases, the lattice parameters expand proportionally. Interestingly, $Ti_{0.9375}Sn_{0.0625}O$ exhibits a higher bulk modulus compared to pure $TiO_2$, indicating greater rigidity. This bulk modulus corresponds to the smallest unit cell volume among the studied Sn concentrations (12.5% and 25%).

**Table 1.** Bulk modulus, lattice constants, and pressure derivative for $Ti_{1-x}Sn_xO$ at different Sn doping concentrations.

| Sn concentration (at.%) | a(Å) | c(Å) | $B_0$(GPa) | B' |
|---|---|---|---|---|
| 0 | 4.658, 4.587[a]<br>4.594[b], 4.653[c]<br>4.567[d], 4.574[e] | 2.987, 2.954[a]<br>2.959[b], 2.965[c]<br>2.933[d], 2.927[e] | 228.1542 | 4.296 |
| 6.25 | 4.421 | 2.355 | 219.1836 | 4.830 |
| 12.5 | 4.476 | 2.686 | 221.5431 | 4.625 |
| 25 | 4.516 | 2.886 | 225.9253 | 4.344 |

[a] Ref. Exp. [25]
[b] Ref. Exp. [26]
[c] Ref. Theo.[27]
[d] Ref. Theo.[28]
[e] Ref. Theo.[29]

## 3.2. ELECTRONIC STRUCTURE

The Becke-Johnson modified (mBJ) exchange functional computes the density of states (DOS) and electronic band structure for pure $TiO_2$ and $Ti_{1-x}Sn_xO$, with $x$ = 0%, 6.25%, 12.5%, and 25%.

Figure 2 shows the band structures and DOS of pure $TiO_2$. According to the computed band structure, In the Brillouin zone, the valence band's (VBM) maximum and the conduction band's (CBM) minimum are located at the same Γ-point. Proving that pure $TiO_2$ is a typical semiconductor with a direct band gap. Regarding pure $TiO_2$, the computed energy gap is 2.73 eV, near the experimental value of 3.0 eV [25], and represents an improvement over previous theoretical estimates [30–32].
Figure 2 illustrates how the valence band splits into two areas: the lower valence band, which extends from -4.69 eV to -2.99 eV and has contributions as high as -18.40 eV, and the upper valence band, which extends from -2.99 eV to -0.07 eV. The O-2p orbital states comprise most valence band edges close to the fixed Fermi energy of 0 eV. On the other hand, Ti-3d orbitals have a minimal impact on the conduction band edges close to the Fermi energy. The O-2p orbitals comprise most of the valence band, which extends from the Fermi level to -2.99 eV, with minor contributions from Ti-3d states. O in its 2p states and Ti in its 3d states comprise most of the lower valence band. Additionally, the valence band at lower mainly comprises the 3d states of Ti and the 2p states of O.

The band structures, both partial and total densities of states (PDOS and TDOS) for Sn-doped $TiO_2$ at different concentrations, are shown in Figures 3, 4, and 5. The conduction band minimum is noticeably higher than in pure $TiO_2$, which causes the optical band gap to grow. At $x$=6.25%,12.5%,x=6.25%,12.5%, and 25%, the optical band gaps determined for $Ti_{1-x}Sn_xO$ are 3.13 eV, 3.18 eV, and 3.73 eV, respectively. This rise in band gap energy with Sn concentration is consistent with experimental findings and other theoretical calculations [33].

Importantly, no new states emerge within the band gap following Sn doping, and the VBM of Sn-doped $TiO_2$ stays the same. The lowest part of the conduction band is shaped by the Sn-5s and Sn-5p orbitals, mainly through the 5s states, which results in the conduction band minimum shifting northward. Furthermore, for all Sn concentrations, localized Sn-5s and Sn-4d orbitals appear in the upper and lower valence bands at approximately -6 eV and -20 eV, respectively.

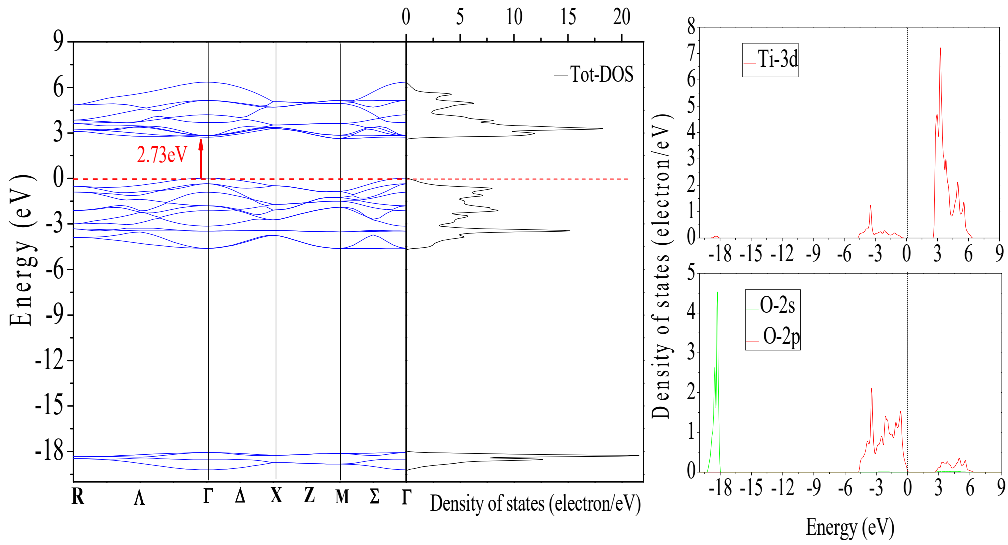


**Figure 2.** Electronic band structure and density of states of pure $TiO_2$.

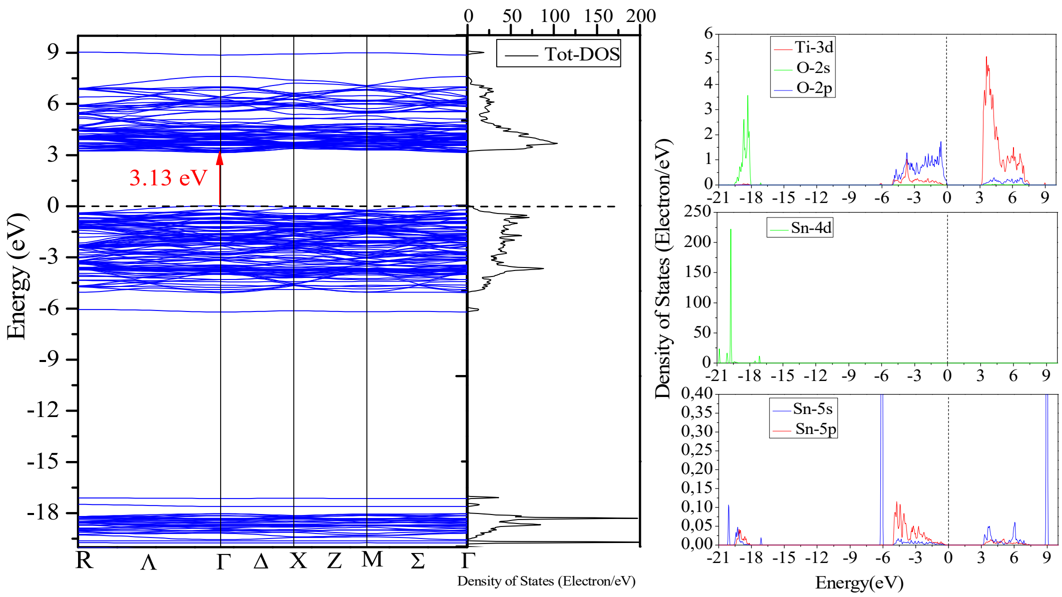


**Figure 3.** Electronic band structure and density of states of $TiSnO_2$ (2x2x2)

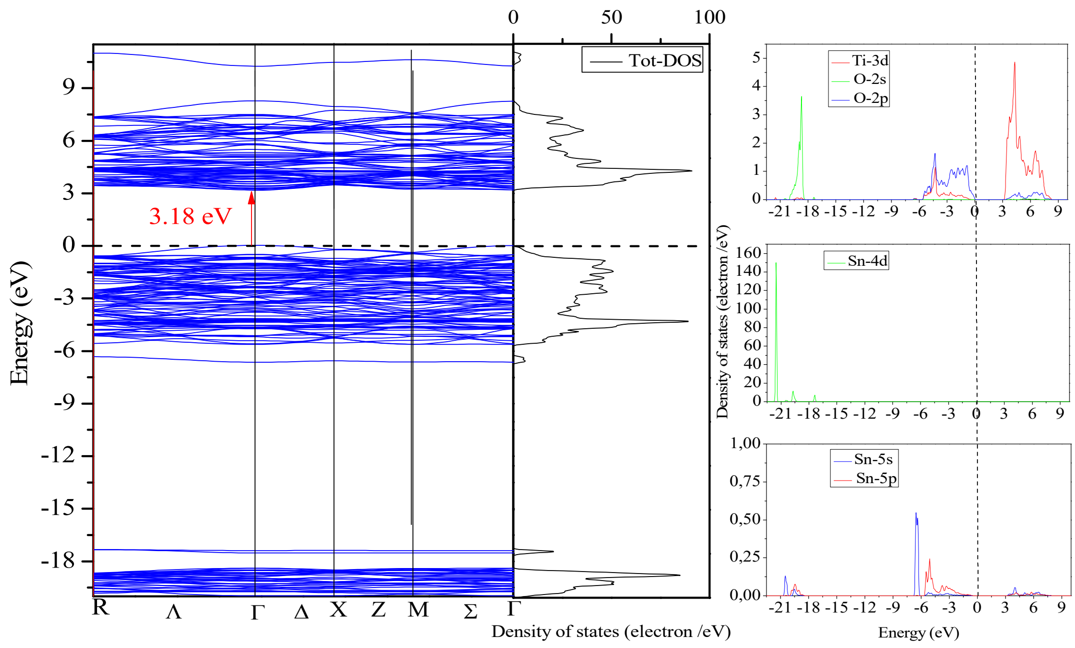

**Figure 4.** Electronic band structure and density of states of $TiSnO_2$ (1x2x2).

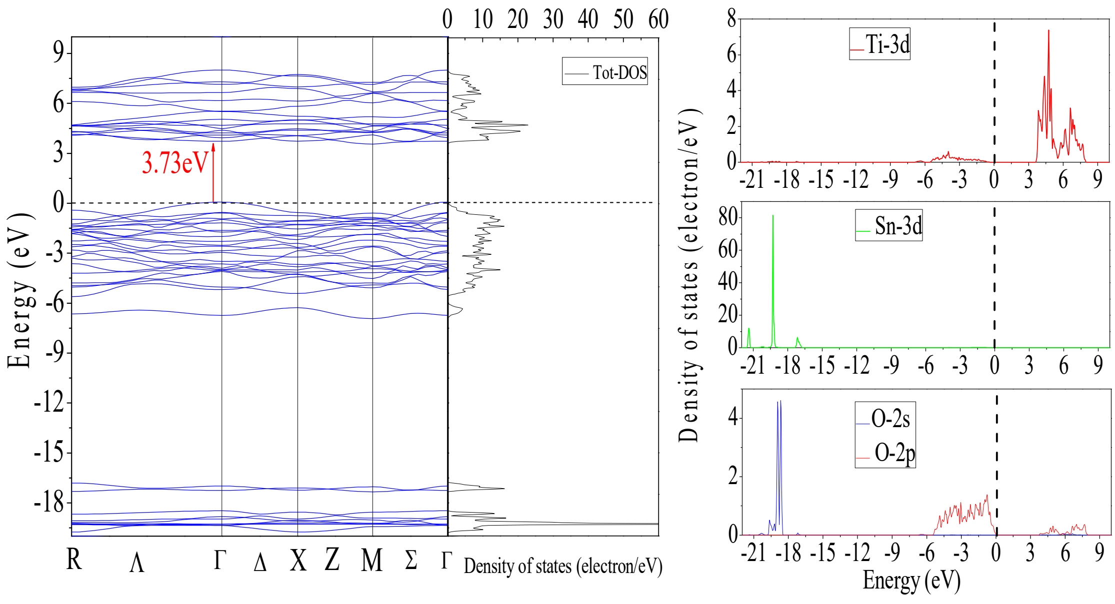

**Figure 5.** Electronic band structure and density of states TiSnO2 (1x1x2).

### 3.2. OPTICAL PROPERTIES

The optical properties of $TiO_2$, both in its pure state and doped with Sn at different concentrations, are described in this section. These properties are defined by the previously determined complex dielectric function $\varepsilon(\omega)$. Figure 6 illustrates the imaginary component $\varepsilon_2(\omega)$ of the dielectric function for pure and Sn-doped $TiO_2$ at various concentrations.

Determining the transitions between occupied states below the Fermi level and unoccupied states above it as a result of photon absorption requires calculating the imaginary portion. Because of the optical anisotropy of the crystal, researchers measure the spectra with the electric field vector parallel to the crystallographic c-axis.

It is clear from Fig. 6 that the band gap value, or the fundamental absorption edge, closely corresponds with the peak in pure $TiO_2$ at about 2.7 eV. This peak results from optical transitions between the conduction band minimum, comprising mixed Ti-3d states ($2t_{2}g$ and $3e_{e}g$), and the valence band maximum, comprised of O-2p states.

Upon doping $TiO_2$ with Sn at various concentrations, the peaks of $\varepsilon_2(\omega)$, shown in Figure 7, become more pronounced within the range of 4.5 eV to 7.5 eV for pure $TiO_2$ (transitions O-2p (t2g) and O-2p (eg) blocks) and decrease with increasing Sn concentration. Additionally, the absorption edge is significantly shifted to higher energies (from 7.5 eV to 25 eV) by Sn doping, and this shift increases with greater Sn concentrations.

The absorptive transitions at the band edge are predominantly associated with transitions from Sn-5p to Ti-3d states rather than from O-2p as in pure $TiO_2$ (transition Sn-5p (t2g) is more important than for the Sn-5p (eg) blocks).

Notably, the transition from Sn-5p to $t_{2}g$ states becomes more significant than the, e.g. states. These findings confirm that Sn atoms effectively enhance UV absorption when doped into the substitutional sites of rutile $TiO_2$.

The optical dielectric function's actual components for pure and Sn-doped rutile $TiO_2$ at varying concentrations are shown in Fig. 7. There are distinct peaks for 0%, 6.25%, 12.5%, and 25% Sn concentrations at 3.31 eV, 3.66 eV, 3.80 eV, and 4.61 eV, respectively.

These peaks correspond to the same transitions noted in $\varepsilon_2(\omega)$; following these peaks, $\varepsilon_1(\omega)$ declines to zero, turns negative, hits a minimum, and then rises again toward 0 and 1 at higher energies.

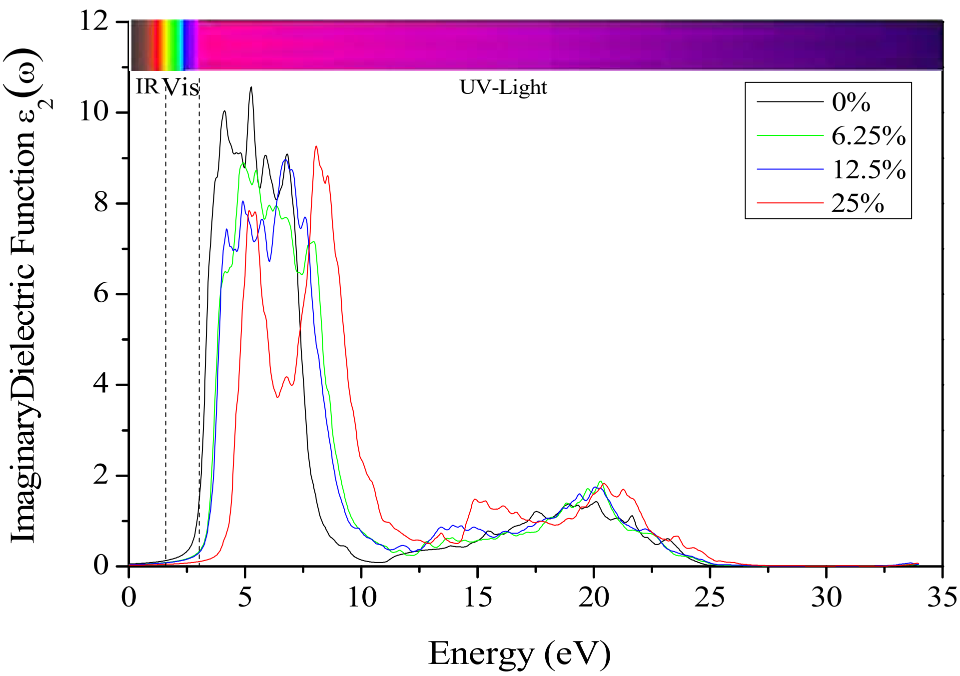


**Figure 6.**The imaginary part of the dielectric function for various $Ti_{1-x}Sn_xO$ concentrations

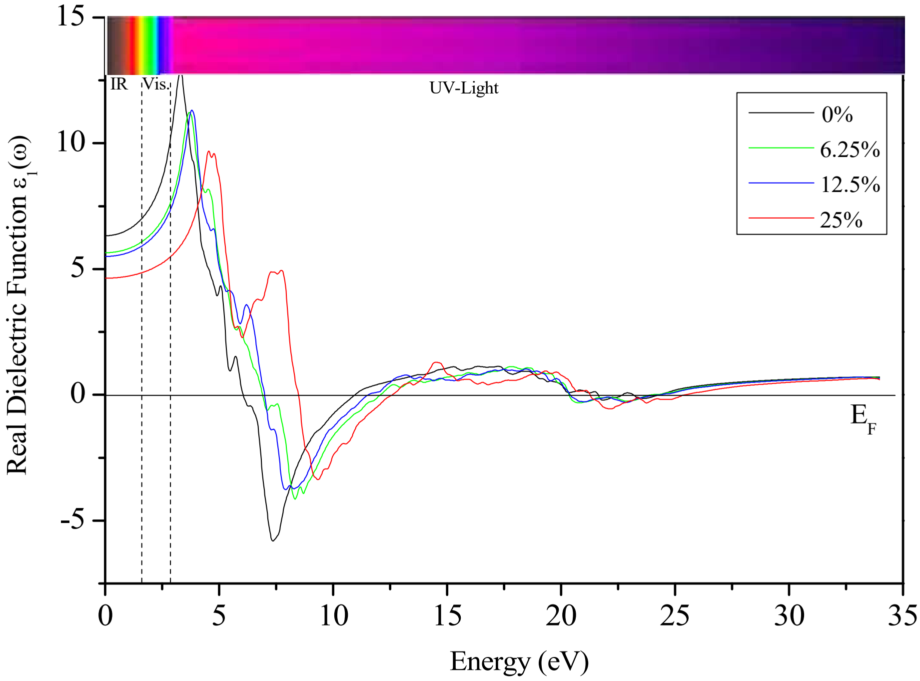


**Figure 7.**The imaginary part of the dielectric function for various $Ti_{1-x}Sn_xO$ concentrations

The optical absorption spectra for pure and Sn-doped $TiO_2$ at different concentrations as a function of energy in Fig. 8. The absorption spectra reveal strong absorption beyond 3 eV (in the UV region) while showing low absorption in the infrared and visible regions. This behaviour aligns well with experimental studies of pure $TiO_2$ thin films [35,36].

The figure shows that within the energy range of 3.5 to 6.7 eV, the absorption spectrum decreases with increasing Sn concentration, with the 25% concentration exhibiting the lowest absorption. Conversely, in the energy range of 7.0 eV to 20 eV, the absorption spectrum increases with higher Sn concentrations, with the 25% sample demonstrating the most substantial absorption. Notably, higher concentrations of Sn introduce new absorption bands around 8.27 eV, 16.65 eV, and 20.93 eV.

Compared to pure $TiO_2$, the Sn-doped $TiO_2$ shows a blue shift in the absorption peak, indicating a change in the material's energy levels as the absorption peak shifts towards higher energies. Additionally, the absorption of Sn-doped $TiO_2$ extends into higher energy ranges (beyond 30 eV) compared to pure $TiO_2$, highlighting the enhanced optical properties conferred by Sn doping.

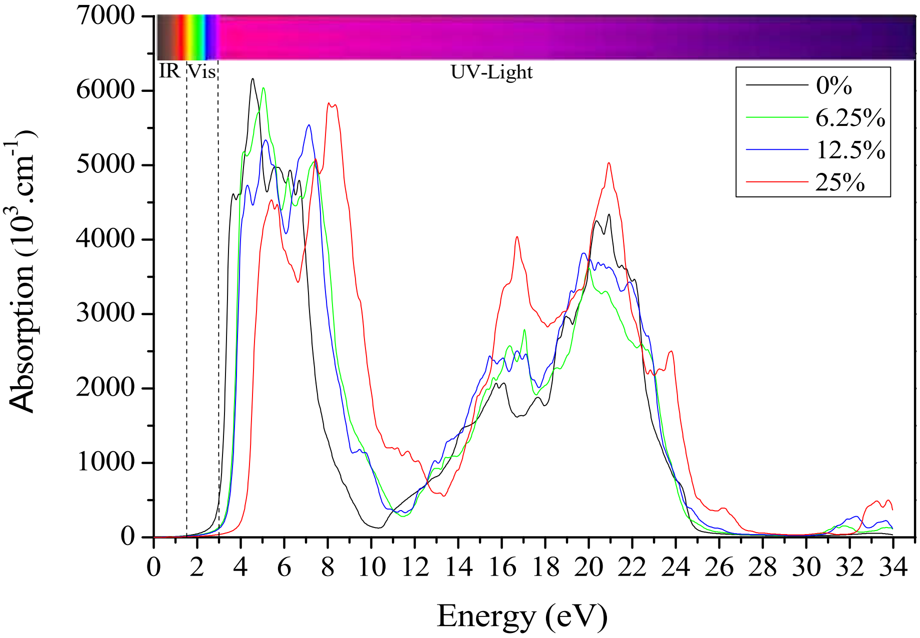


**Figure 8.**The change of the absorption for various $Ti_{1-x}Sn_xO$ concentrations.

Fig. 9 illustrates the Reflectivity as a function of energy.
(eV) for both pure and Sn-doped $TiO_2$. Pure $TiO_2$ displays low Reflectivity in the visible and infrared regions, remaining below 0.3%. Reflectivity increases significantly in the visible region just before reaching the UV edge, peaking at 0.6% at 9.57 eV (first peak). Following this peak, Reflectivity declines to less than 0.1% up to approximately 22 eV, then rises again to around 0.35% at 25 eV (second peak) before dropping nearly to 0% at higher energies.

Incorporating Sn ions into the $TiO_2$ structure results in lower Reflectivity than pure $TiO_2$ up to 16 eV. Specifically, the Reflectivity decreases for energies ranging from 0 to 16 eV. At zero energy, we record the following reflectivity values: 0.16 for $x$ = 0%, 0.15 for $x$ = 6.25%, 0.14 for $x$ = 12.5%, and 0.11 for $x$ = 25%. This trend highlights the significant impact of Sn doping on the optical reflectivity properties of our material.

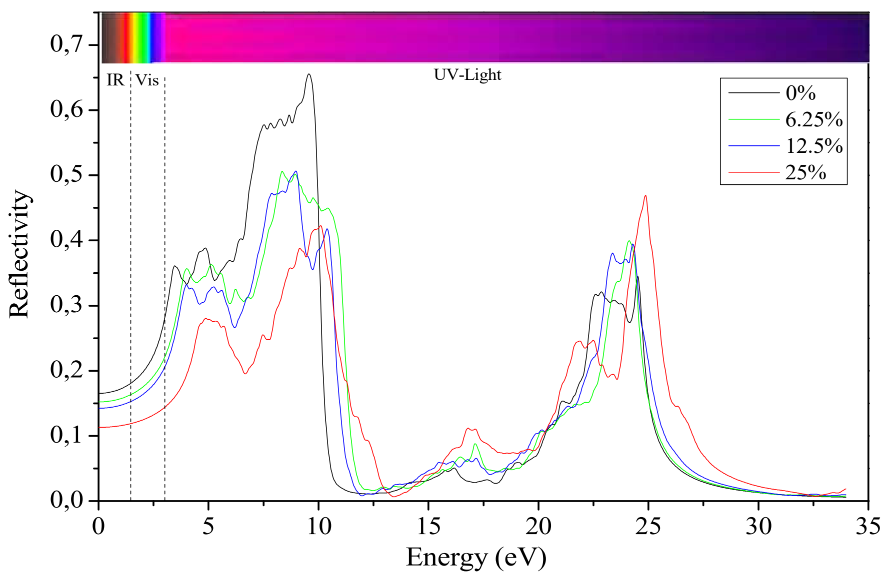


**Figure 9.**The change of the Reflectivity for various $Ti_{1-x}Sn_xO$ concentrations.

The electron energy loss function L(ω), which depicts the energy losses incurred by a rapid electron moving through the material, is shown in Fig. 10. The primary peak of the L(ω) curve indicates the volume plasma frequency $\omega_p$, occurring when $\varepsilon_1(\omega)$ reaches zero and $\varepsilon_2(\omega) <1$ [37]. We locate the peak of the L(ω) function for pure $TiO_2$ at 25.18 eV, and it decreases as Sn concentration increases.

This reduction in the peak indicates a significant decrease in energy loss, highlighting the importance of Sn doping. At 25% Sn concentration, the energy loss peak shifts from 25 eV to 28.13 eV, indicating that the metallic properties persist up to 28 eV.

The prominent peak in L(ω) reflects the metallic nature of pure $TiO_2$, which is greater than that of Sn-$TiO_2$. The variance in L(ω) response is ascribed to the uniform distribution of Ti ions in pure $TiO_2$, resulting in enhanced structural order.

In contrast, Sn-doped $TiO_2$ shows increased disorder due to two distinct metallic ions (Ti and Sn), resulting in increased energy losses among ions possessing distinct electrical and physical characteristics.

The peak positions in the loss spectra indicate the transition of $\varepsilon_1(\omega)$ from positive to negative values, signifying a shift from metallic to dielectric characteristics. Additionally, we observe occupied states in Sn-doped $TiO_2$ from a second peak around 11 eV.

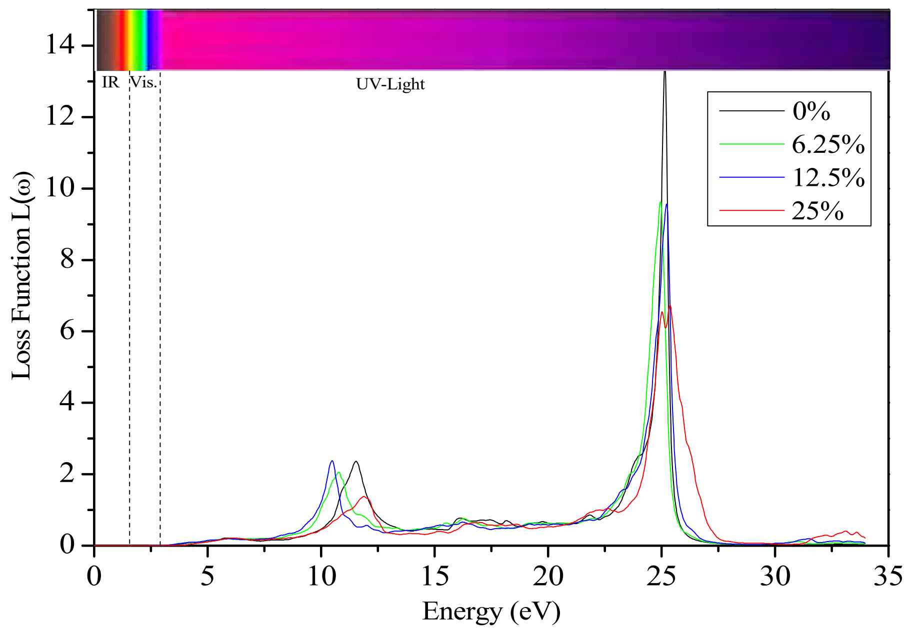


**Figure 10.**The change of the Energy Loss for various $Ti_{1-x}Sn_xO$ concentrations.

**4. CONCLUSION**

This ab initio study, utilizing the Local Orbital plus Full Potential Linearized Augmented Plane-Wave (FP-(L)APW+lo) method and DFT, or density functional theory with the modified Becke–Johnson (mBJ) exchange potential, provides comprehensive insights into the effects of Sn doping on rutile $TiO_2$. We observe significant modifications in the structural stability, electronic structure, and optical properties of pure $TiO_2$ and Sn-doped $TiO_2$ at various concentrations.

The optimized lattice constants, bulk modulus, and pressure derivative for pure $TiO_2$ align well with theoretical and experimental values. Sn doping induces notable changes in the crystal structure, particularly at higher concentrations, affecting the overall stability of the material. The electronic band structure and density of states are significantly altered by Sn doping, with the calculated energy gap for pure $TiO_2$ being 2.73 eV, demonstrating a minimal deviation of 0.91% from the experimental value.

Doping with Sn increases the optical band gap, with values rising from 3.13 eV to 3.73 eV as Sn concentration increases. Sn introduces defect states without affecting the position of the valence band maximum but shifts the conduction band minimum upward due to contributions from Sn-5s and Sn-5p orbitals.

The optical properties, analyzed through the complex dielectric function, show enhanced UV absorption for Sn-doped $TiO_2$, shifting the absorption edge to higher energies and increasing absorption strength at higher Sn concentrations. The absorption spectra and reflectivity data indicate improved UV absorption and reduced Reflectivity in the visible region for doped samples.

The energy loss function reveals a significant reduction in energy loss with increasing Sn concentration, suggesting lower energy losses and highlighting the effectiveness of Sn doping in altering the material's properties. Higher Sn concentrations also indicate a shift towards metallic behaviour at elevated energy levels.

The findings confirm that Sn doping in rutile $TiO_2$ effectively modifies its structural, electronic, and optical properties. These findings make it a viable and potentially cost-effective alternative to traditional Transparent Conductive Oxide (TCOs) like indium-doped tin oxide (ITO). This enhancement positions Sn-doped $TiO_2$ as a promising candidate for applications in solar cells, photocatalysis, and other optoelectronic devices where transparency and conductivity are crucial.

***Acknowledgements***

The Ministry of Higher Education and Scientific Research of Algeria, through the PRFU project N°A11N01UN130120230009, generously supported the successful completion of this research. This backing has been invaluable in facilitating a comprehensive investigation into the effects of Sn doping on $TiO_2$. We sincerely appreciate the resources, funding, and institutional support that have significantly contributed to advancing knowledge in this field. The collaboration and encouragement throughout this project have been crucial in achieving the research objectives.

**References**

[1] M. Grätzel, J.Photochem.Photobiol.C4(2003)145.
[2] B. O'Regan, M.Grätzel,Nature353(1991)737.
[3] X.B. Chen,S.S.Mao,Chem.Rev.107(2007)2891.)
[4] W. Maziarz, A. Kusior, A. Trenczek-Zajac, Gaz sensing.Nanostructured TiO2-based gas sensors with enhanced sensitivity to reducing gases, Beilstein J. Nanotechnol. 7 (2016) 1718–1726.
[5] B. Sun, T. Shi, Z. Peng, W. Sheng, T. Jiang, G. Liao, Controlled fabrication of Sn/ TiO2nanorods for photoelectrochemical water splitting, Nanoscale Res. Lett. 8 (2013) 1–8.
[6] C. Han, R. Luque, D. Dionysiou, Facile preparation of controllable size monodisperse anatase titania nanoparticles, Chem. Comm. 48 (2012) 1856–1862.
[7] Y. Cai, H.E. Wang, S.Z. Huang, M.F. Yuen, H.H. Cai, C. Wang, Y. Yu, Y. Li, W.J. Zhang, B.L. Su,
Porous TiO2 urchins for high-performance Li_ion battery electrode: facile synthesis, characterization and structural evolution, Electrochem. Acta 210 (2016) 206–214.
[8] B. Tan, Y.Y. Wu, Dye-sensitized solar cells based on anatase TiO2nanoparticles/ nanowires composites, J. Phys. Chem. B 110 (2006) 15932–15938.
[9] H. Tang, F. Lévy, H. Berger, P.E. Schmid, Phys. Rev. B 52 (1995) 7771.
[10] F. Arntz, Y. Yacoby, Phys. Rev. Lett. 17 (1966) 857.
[11] De Angelis, F.; Di Valentin, C.; Fantacci, S.; Vittadini, A.; Selloni, A. Theoretical Studies on Anatase
and Less Common TiO2 phases: Bulk, Surfaces, and Nanomaterials Chem. Rev. 2014, 114, 9708–9753 DOI: 10.1021/cr500055q
[12] Mingzheng Ge, Jingsheng Cai, James Iocozzia, Chunyan Cao, Jianying Huang, Xinnan Zhang, Jiali Shen, Shanchi Wang, Songnan Zhang, Ke-Qin Zhang, Yuekun Lai, Zhiqun Lin, A review of TiO2 nanostructured catalysts for sustainable H2 generation, Int. J. Hydrogen Energy 42 (2017) 8418–8449.
[13] O. Carp, C. L. Huisman, and A. Reller, "Photoinduced reactivity of titanium dioxide," Progress in Solid State Chemistry, vol. 32, no. 1-2, pp. 33–177, 2004. View at Publisher · View at Google

Scholar · View at Scopus
[14] A. Kitiyanan and al., "The preparation and characterization of nanostructured TiO2-ZrO2 mixed oxide electrode for efficient dye-sensitized solar cells," Journal of Solid State Chemistry, vol. 178, no. 4, pp. 1044–1048, 2005. View at Publisher · View at Google Scholar · View at Scopus
[15] M. Dürr, S. Rosselli, A. Yasuda, and G. Nelles, "Band-gap engineering of metal oxides for dye-sensitized solar cells," Journal of Physical Chemistry B, vol. 110, no. 43, pp. 21899–21902, 2006. View at Publisher · View at Google Scholar · View at PubMed · View at Scopus
[16] J. Li and H. C. Zeng, "Hollowing Sn-doped TiO2 nanospheres via Ostwald ripening," Journal of the American Chemical Society, vol. 129, no. 51, pp. 15839–15847, 2007. View at Publisher · View at Google Scholar · View at PubMed · View at Scopus
[17] (a) S. Mahanty, S. Roy, S. Sen, Effect of Sn doping on the structural and optical properties of sol-gel TiO2 thin films, J. Cryst. Growth 261 (2004) 77; (b) H. Sayilkan, Appl. Catal. A 319 (2007) 230.
[18] Madsen G K H, Blaha P, Schwarz K, Sjöstedt E and Nordström L 2001 Efficient linearization of the augmented plane-wave method Phys. Rev. B 64 195134
[19] Khon W and Sham L J 1965 Self-consistent equations including exchange and correlation effects Phys. Rev. 140 A1133
[20] Perdew J P, Burke K and Ernzerhof M 1996 Generalized gradient approximation made simple Phys. Rev. Lett. 77 3865
[21] Tran F and Blaha P 2009 Accurate band gaps of semiconductors and insulators with a semilocal exchange-correlation potential Phys. Rev. Lett. 102 226401
[22] J. Sun, H. Wang, J. He, Y. Tian, Phys. Rev. B 71 (2005) 123132.
[23] F. Wooten, Optical Properties of Solids, Academic, New York, 1972.
[24] J. Sun, H. Wang, J. He, Y. Tian, Phys. Rev. B 71 (2005) 123132
[25] J.K. Burdett, T. Hughbanks, G.J. Miller, J.W. Richardson, J.V. Smith, J. Am. Chem.Soc. 109 (1987) 3639.
[26] S.C. Abrahams, J.L. Bernstein, J. Chem. Phys. 55 (1971) 3206.
[27] K.M. Glassford, J.R. Chelikowsky, Phys. Rev. B 46 (1992) 1284.
[28] R. Sikora, J. Phys. Chem. Solids 66 (2005) 1069.
[29] J. Muscat, V. Swamy, N.M. Harrison, Phys. Rev. B 65 (2002) 224112.
[30] Y.-z. Fang et al. Chinese Journal of Physics 56 (2018) 1370–1377
[31] R. Long et al. / Computational Materials Science 45 (2009) 223–228
[32] C. Di Valentin, G. Pacchioni, A. Selloni, Phys. Rev. B 70 (2004) 085116
[33] R. Long, Y. Dai, G. Menga, B. Huanga , Phys. Chem. Chem. Phys., 11(2009) 8165.
[34] J. Li, H. C. Zeng, J. Am. Chem. Soc., 129 (2007) 15839.
[35] A.H. Mayabadi et al. / Journal of Physics and Chemistry of Solids 75 (2014) 182–187
[36] S. E. H. Yeganeh et al./Journal of Materials Science, Materials in Electronics (2018)10841–10852
[37] H. I. Berrezoug, A. E. Merad, M. Aillerie and A. Zerga 2017, First principle study of structural stability, electronic structure and optical properties of Ga doped ZnO with different concentrations, Mater. Res. Express 4 (2017) 035901.